

Joint Constraints on the Hubble Constant, Spatial Curvature, and Sound Horizon from the Late-time Universe with Cosmography

KAITUO ZHANG,¹ TIANYAO ZHOU,¹ BING XU,² QIHONG HUANG,³ AND YANGSHENG YUAN^{4,5,6}

¹*Department of Physics, Anhui Normal University, Wuhu, Anhui 241000, China*

²*School of Electrical and Electronic Engineering, Anhui Science and Technology University, Bengbu, Anhui 233030, China*

³*School of Physics and Electronic Science, Zunyi Normal University, Zunyi 563006, Guizhou, China*

⁴*Shandong Provincial Engineering and Technical Center of Light Manipulations and Shandong Provincial Key Laboratory of Optics and Photonic Device, School of Physics and Electronics, Shandong Normal University, Jinan 250014, China;*

⁵*Collaborative Innovation Center of Light Manipulation and Applications, Shandong Normal University, Jinan 250358, China;*

⁶*Joint Research Center of Light Manipulation Science and Photonic Integrated Chip of East China Normal University and Shandong Normal University, East China Normal University, Shanghai 200241, China;*

ABSTRACT

In this paper, using the latest Pantheon+ sample of Type Ia supernovae (SNe Ia), Baryon Acoustic Oscillation (BAO) measurements, and observational Hubble data (OHD), we carry out a joint constraint on the Hubble constant H_0 , the spatial curvature Ω_K , and the sound horizon at the end of drag epoch r_d . To be model-independent, four cosmography models, i.e., the Taylor series in terms of redshift $y_1 = z/(1+z)$, $y_2 = \arctan(z)$, $y_3 = \ln(1+z)$, and the Padé approximants, are used without the assumption of flat Universe. The results show that the H_0 is anti-correlated with Ω_K and r_d , indicating smaller Ω_K or r_d would be helpful in alleviating the Hubble tension. And the values of H_0 and r_d are consistent with the estimate derived from the Planck Cosmic Microwave Background (CMB) data based on the flat Λ CDM model, but H_0 is in $2.3\sim 3.0\sigma$ tension with that obtained by [Riess et al. \(2022\)](#) in all these cosmographic approaches. Meanwhile, a flat Universe is preferred by the present observations under all approximations except the third order of y_1 and y_2 of the Taylor series. Furthermore, according to the values of the Bayesian evidence, we found that the flat Λ CDM remains to be the most favored model by the joint datasets, and the Padé approximant of order (2,2), the third order of y_3 and y_1 are the top three cosmographic expansions that fit the datasets best, while the Taylor series in terms of y_2 are essentially ruled out.

1. INTRODUCTION

In modern cosmology, the Hubble tension has become one of the most prominent issues. The Hubble constant H_0 , as a fundamental cosmological parameter, represents the expansion rate of the present Universe, which can be obtained by both global and local measurements, i.e., based on the standard cosmological model (Λ CDM), Planck Collaboration inferred $H_0 = 67.4 \pm 0.5 \text{ km s}^{-1} \text{ Mpc}^{-1}$ (hereafter P18) ([Planck Collaboration et al. 2020](#)) from Planck satellite measurements of Cosmic Microwave Background (CMB) temperature and polarization anisotropies, while, Supernovae and H_0 for the Equation of State of dark energy (SH0ES) collaboration found $H_0 = 73.04 \pm 1.04 \text{ km s}^{-1} \text{ Mpc}^{-1}$ (hereafter R22) ([Riess et al. 2022](#)) via local measurements from type Ia supernovae (SNe Ia) calibrated by the distance ladder without any cosmological model. The 5σ tension between these two independent H_0 estimates could be pointing towards new physics beyond the standard model or residual systematics ([Freedman 2017](#); [Feeney et al. 2018](#); [Di Valentino et al. 2018](#); [Handley 2021](#)). To alleviate the discrepancy, fundamental physics beyond Λ CDM are investigated, such as time-dependent dark energy equation of state ([Huang & Wang 2016](#); [Di Valentino et al. 2016, 2021](#); [Zhao et al. 2017](#); [Miao & Huang 2018](#); [Yang et al. 2019](#); [Poulin et al. 2019](#); [Vagnozzi et al. 2021](#); [Colgáin et al. 2021](#); [Yang et al. 2023](#)), modified gravity ([Capozziello et al. 2003](#); [Nunes 2018](#); [Farrugia et al. 2021](#); [Koussour et al. 2022](#); [Sultana et al. 2022](#)), and additional relativistic particles, see [Kumar & Nunes \(2016\)](#); [Xu & Huang \(2018\)](#); [Carneiro et al. \(2019\)](#); [Pandey et al. \(2020\)](#); [D'Eramo et al. \(2022\)](#). Alternately, new approaches to determine the

Hubble constant from local direct measurements are proposed. For example, through time-delay cosmography, the H_0 Lenses in COSMOGRAIL’s Wellspring (H0LiCOW) Collaboration (Suyu et al. 2017) measured the Hubble constant from strong gravitational lens systems with time delays between the multiple images. Using detected gravitational waves (GW) as a ‘standard siren’, binary neutron-star (BNS) system detection GW170817 and subsequent observations in the electromagnetic (EM) domain provide another independent method of measuring the Hubble constant (Abbott et al. 2017). Adopting revised measurement, Freedman et al. (2020) found $H_0 = 69.9 \pm 0.8(\pm 1.1\% \text{ stat}) \pm 1.7(\pm 2.4\% \text{ sys}) \text{ km s}^{-1} \text{ Mpc}^{-1}$, which provided one of the most accurate means of measuring the distances to nearby galaxies by the red giant branch method.

However, if the systematic uncertainties are not the main drivers of H_0 tension, then the discrepancy coming from the concrete cosmological model assumption can not be ignored. In order to extricate from dependency on a cosmological model and study the expansion of the Universe directly from the observations, various model-independent techniques are used, such as cosmography, the Bézier parametric curve, the Parameterization based on cosmic Age (PAge), the Gaussian process (GP) method and so on (Wojtak & Agnello 2019; Capozziello et al. 2019; Yang et al. 2020; Zhang & Huang 2021; Cai et al. 2022a,b; Hu & Wang 2022; Jalilvand & Mehrabi 2022; Liu et al. 2022). For examples, Zhang & Huang (2021) reconstructed $H(z)$ in cubic expansion and polynomial expansion respectively, and constrained H_0 and r_d with the joint data of SNe Ia, Baryon Acoustic Oscillation (BAO) measurements, Observational Hubble Data (OHD), and GW data, and found the H_0 value is in 2.4-2.6 σ tension with SH0ES 2019 (Riess et al. 2019). Cai et al. (2022a,b) applied the PAge approximation to consistently use the OHD and the late-time matter perturbation growth data at high redshifts, and found the Hubble tension can’t be solved by introducing the new physics at the late time beyond the Λ CDM model. Hu & Wang (2022) investigated the redshift-evolution of H_0 with 36 Hubble parameter $H(z)$ data based on the GP method, and found there was a late-time transition of H_0 which effectively alleviated the Hubble crisis by 70%. It should be pointed out that these works are all taken under the assumption of a spatially flat Universe. However, there is still one observational probe that is in agreement with a negative curvature, sparking the debate about the flatness of the Universe. From the combination of CMB temperature and polarization power spectra, the constraint on curvature suggests a closed Universe at more than three standard deviations ($\Omega_K = -0.044_{-0.015}^{+0.018}$) (Planck Collaboration et al. 2020). Whereas once the Planck CMB data are combined with the BAO measurements, a flat Universe is preferred with a high precision $\Omega_K = 0.001 \pm 0.002$ (Planck Collaboration et al. 2020), indicating there is a discrepancy between CMB and BAO data for the constraint on Ω_K , namely ‘‘curvature tension’’ (Handley 2021). As allowing for spatial curvature may significantly affect constraints on cosmological parameters (Dossett & Ishak 2012), the curvature parameter also needs to be considered when exploring Hubble tension. For instance, it is found that a negative curvature preferred by P18 will exacerbate H_0 tension (Di Valentino et al. 2020, 2021), while Wang et al. (2021) and Cao et al. (2022) found that a spatially flat Universe is favored using the mock GW data in combination with the Hubble parameter or strong gravitational lensing time delay (SGLTD) data respectively. Therefore, due to the significant influence of spatial curvature on the H_0 measurement and the inconsistency of the spatial curvature measurement, it is very necessary for us to measure H_0 with various observations under the assumption of a non-flat Universe.

Additionally, since that the value of H_0 obtained from the Planck CMB data is directly tied to the sound horizon at last scattering, which is closely related to the sound horizon r_d at the baryon decoupling, a number of amendments to the Λ CDM model have been proposed, aiming to release the Hubble tension by reducing r_d and increasing H_0 (Karwal & Kamionkowski 2016; Buen-Abad et al. 2018; Anchordoqui & Bergliffa 2019; Niedermann & Sloth 2020; Berghaus & Karwal 2020; Archidiacono et al. 2020). However, the most recent works demonstrated that any model which only reduces r_d can never fully resolve the Hubble tension (Pogosian et al. 2020; Jedamzik et al. 2021). In addition, in order to break the measured degeneracy between r_d and H_0 , many works have therefore attempted to measure the H_0 and r_d by combining the BAO measurements with other late-time observations of Universe. For instance, Wojtak & Agnello (2019) combined BAO with the SGLTD, Joint Light-Curve Analysis (JLA), and the reconstructed $H(z)$ data via the polynomial expansion, and obtained $H_0 = 72.3 \pm 6.9 \text{ km s}^{-1} \text{ Mpc}^{-1}$, $r_d = 139.2 \pm 13.3 \text{ Mpc}$. Then Pogosian et al. (2020) found $r_d = 143.7 \pm 2.7 \text{ Mpc}$ and $H_0 = 69.6 \pm 1.8 \text{ km s}^{-1} \text{ Mpc}^{-1}$ by using the latest BAO data along with a $\Omega_m h^2$ prior based on the Planck best-fit Λ CDM model, and similar values were obtained when they combined BAO with the Pantheon supernovae, the Dark Energy Survey Year 1 galaxy weak lensing (Abbott et al. 2018), Planck/SPTP01 CMB lensing, and OHD. In addition, Cai et al. (2022b) combined the SNe Ia, BAO and OHD, and obtained $H_0 = 68.958_{-1.826}^{+1.779} \text{ km s}^{-1} \text{ Mpc}^{-1}$ and $r_d = 146.466_{-3.302}^{+3.448} \text{ Mpc}$ by using the PAge approximation. Although the Hubble tension can be alleviated in these works, it cannot be completely resolved. To reflect the reality

of these works taken under the assumption of a spatially flat Universe, it is well worth constraining H_0 and r_d with leaving Ω_K free by using the latest low-redshift observational data.

In this work, we therefore plan to carry out a joint constraint on H_0 , Ω_K and r_d with the latest late-time observations of Universe including SNe Ia, BAO, and OHD. Specially, the newest Pantheon+ sample of SNe Ia (Brout et al. 2022; Scolnic et al. 2022) ranging in redshift from $z = 0.001$ to 2.26, is used. This sample is made of 1701 light curves of 1550 spectroscopically confirmed SNe Ia and significantly enlarges the origin Pantheon sample size from the addition of multiple cross-calibrated photometric systems of SNe Ia. For the BAO measurements, fourteen latest measurements of $D_V(z)/r_d$, $D_M(z)/r_d$ and $D_H(z)/r_d$ summarized in Ref. (Alam et al. 2021), covering the redshift range $0.15 \leq z \leq 2.33$, are used. These data are obtained from final observations of clustering using galaxies, quasars, and Ly α forests from the completed SDSS lineage of experiments in a large-scale structure, composing of data from SDSS, SDSS-II, BOSS and eBOSS. Furthermore, to be model-independent, the well-consolidated approach named cosmography (Chiba & Nakamura 1998; Caldwell & Kamionkowski 2004; Visser 2004, 2005, 2015; Capozziello et al. 2013, 2019; Dunsby & Luongo 2016; Zhang et al. 2017; Yin & Wei 2019; Li et al. 2020) is used, which has attracted lots of attention in the study of the expansion of Universe. The idea of cosmography is to expand the cosmological distances or the Hubble parameter into a Taylor series of redshift z , which performs well at low redshifts but encounters the convergence problems in the high-redshift domain (Cattoën & Visser 2007). To overcome the convergence issues, several improved approaches have been proposed, one of which relies on the use of auxiliary variables (Cattoën & Visser 2007; Aviles et al. 2012; Capozziello et al. 2020), and the other expands observables in terms of rational approximations (Gruber & Luongo 2014; Wei et al. 2014; Shafieloo 2012; Capozziello et al. 2018). Recently, Li et al. (2020) adopted two cosmographic methods, the Taylor series in terms of $y = z/(1+z)$ and Padé polynomials, to investigate the spatial curvature parameter with the dataset including the Pantheon sample of SNe Ia, BAO, and OHD data, and found the H_0 tension problem can be slightly relaxed by introducing the spatial curvature parameter. In order to get more robust results, we explore the Hubble tension through the extended cosmographic techniques with Taylor series in terms of $y_1 = z/(1+z)$, $y_2 = \arctan(z)$, $y_3 = \ln(1+z)$ and Padé approximations using the latest data, while leaving Ω_K and r_d free at the same time. Meanwhile, a Bayesian approach based on Bayesian evidence is applied to test which cosmographic method is most favored by the observational data.

This paper is organized as follows: In Section 2, we introduce the cosmographic approaches, dataset, and methodology used in this work. In Section 3, our constraint results and analysis are presented. Finally, the conclusions are drawn in Section 4.

2. METHODOLOGY AND DATA

The cosmographic approach is an artful combination of kinematic parameters via the Taylor series with the assumption of large-scale homogeneity and isotropy, which can be retained in the Friedmann–Robertson–Walker (FRW) metric,

$$ds^2 = -c^2 dt^2 + a^2(t) \left[\frac{dr^2}{1 - Kr^2} + r^2(d\theta^2 + \sin^2\theta d\phi^2) \right], \quad (1)$$

where c is the speed of light, K is the constant curvature of the three-space of the FRW metric, and $a(t)$ is the scale factor with cosmic time t . Considering a photon traveling towards us along a radial path ($ds = 0$), we can get

$$cdt = a(t) \frac{dr}{\sqrt{1 - Kr^2}}. \quad (2)$$

Integrating the equation, the comoving distance can be obtained by

$$d_c \equiv a_0 \int_0^{r_e} \frac{dr}{\sqrt{1 - Kr^2}} = -a_0 \int_{t_e}^{t_0} \frac{cdt}{a(t)}, \quad (3)$$

where t_0 and a_0 are the time and scale factor when the photon was observed from us, and t_e is the time when it was emitted from the source at $r = r_e$. Substituting $1 + z = a_0/a$, then the comoving distance becomes

$$d_c = \frac{c}{H_0} \int_0^z \frac{dz'}{E(z)}, \quad (4)$$

where $E(z) \equiv H(z)/H_0$, and the transverse comoving distance (Hogg 1999) can be expressed by

$$D_M(z) = \begin{cases} \frac{c}{H_0\sqrt{\Omega_K}} \sinh\left(\frac{H_0\sqrt{\Omega_K}}{c}d_c\right), & K < 0 \\ d_c, & K = 0 \\ \frac{c}{H_0\sqrt{-\Omega_K}} \sin\left(\frac{H_0\sqrt{-\Omega_K}}{c}d_c\right), & K > 0 \end{cases} \quad (5)$$

where $\Omega_K = -Kc^2/(a_0H_0)^2$ is the present value of spatial curvature parameter. Now define the cosmographic parameters, i.e., Hubble parameter H , deceleration q , jerk j , snap s and lerk l parameters, as follows,

$$\begin{aligned} H(t) &\equiv \frac{1}{a} \frac{da}{dt}, \quad q(t) \equiv -\frac{1}{aH^2} \frac{d^2a}{dt^2}, \quad j(t) \equiv \frac{1}{aH^3} \frac{d^3a}{dt^3}, \\ s(t) &\equiv \frac{1}{aH^4} \frac{d^4a}{dt^4}, \quad l(t) \equiv \frac{1}{aH^5} \frac{d^5a}{dt^5}. \end{aligned} \quad (6)$$

We can expand $D_M(z)$ up to the fifth order,

$$D_M(z) = \frac{c}{H_0} \sum_{i=1}^5 d_i z^i, \quad (7)$$

where

$$\begin{aligned} d_1 &= 1, \\ d_2 &= -\frac{1}{2}(1 + q_0), \\ d_3 &= \frac{1}{6}(2 + 4q_0 + 3q_0^2 - j_0 + \Omega_K), \\ d_4 &= \frac{1}{24}[-6 - 18q_0 + 27q_0^2 + 15q_0^3 + j_0(9 + 10q_0) + s_0 \\ &\quad - 6\Omega_K(1 + q_0)], \\ d_5 &= \frac{1}{120}[24 + 10j_0^2 - l_0 + 96q_0 + 216q_0^2 + 240q_0^3 + 105q_0^4 \\ &\quad - j_0(72 + 160q_0 + 105q_0^2) - 16s_0 - 15q_0s_0 + 5\Omega_K(7 - 2j_0 \\ &\quad + 14q_0 + 9q_0^2) + \Omega_K^2], \end{aligned} \quad (8)$$

with the subscript “0” denoting the values at the present time. Obviously, the $H(z)$ can be expanded directly with the cosmographic parameters, but the expansion is independent of Ω_K . In order to expand $H(z)$ with Ω_K included and improve the usefulness of OHD, we obtain the Hubble function in terms of Ω_K and $D_M(z)$,

$$H(z, \Omega_K) = \frac{c}{\partial D_M(z)/\partial z} \sqrt{1 + \frac{H_0^2 \Omega_K}{c^2} D_M(z)^2}. \quad (9)$$

However, [Cattoën & Visser \(2007\)](#) showed that z -based expansions must break down for $z > 1$. In order to avoid the convergent problem at high redshifts, improved cosmographic techniques have been proposed, namely the auxiliary y -variables and Padé approximations. A fairly well-known y variable is given by

$$y_1 = \frac{z}{1+z}, \quad (10)$$

which is proposed by [Cattoën & Visser \(2007\)](#) and well performed all the way back to the big bang with a nice finite range $[0, 1)$ for $z \in [0, \infty)$. Moreover, in the work [Aviles et al. \(2012\)](#), another parametrization

$$y_2 = \arctan z, \quad (11)$$

is adopted, which behaves smoothly with the arctangent function. It has been demonstrated that y_2 can give well-defined limits $[0, \frac{\pi}{2})$ in the range of $z \in [0, \infty)$ (Aviles et al. 2012). Besides, the third parametrization

$$y_3 = \ln(1 + z), \quad (12)$$

is introduced by Semiz & Kazım Çamlıbel (2015). As a natural logarithmic function, y_3 tends to infinity as $z \rightarrow \infty$, but it increases slowly with the redshift growing.

In addition to the conventional methodology of cosmography applying Taylor expansions of observables, Gruber & Luongo (2014) employed Padé approximants which have the superior convergence properties. For a given function $f(z)$, the Padé approximant of order (m, n) is given by

$$P_{mn}(z) = \frac{a_0 + a_1z + a_2z^2 + \dots + a_mz^m}{1 + b_1z + b_2z^2 + \dots + b_nz^n}, \quad (13)$$

where m and n are non-negative integers, and a_i and b_i are constant that satisfy the conditions $P_{mn}(0) = f(0)$, $P'_{mn}(0) = f'(0), \dots, P^{m+n}_{mn} = f^{m+n}(0)$. According to the plots of the transverse comoving distance $D_M(z)$ and Hubble parameter $H(z)$ for the third-, fourth- and fifth-order Padé approximants in Figure 1 of the work Li et al. (2020), the P_{12} , P_{22} , P_{13} , P_{32} expansions can give good approximations to the Λ CDM model over the redshift interval $z < 2.4$ while other expansions will diverge from Λ CDM model outside a low redshift region.

In this work, we adopt these three parameterizations of Taylor series as well as the Padé approximants to reconstruct the expansion evolution of the Universe and constrain H_0 , Ω_K and r_d . In order to achieve high accurate performance without introducing too many model parameters, the third-, fourth- and fifth-order approximants, namely $y_i^{(j)}$ ($i=1,2,3$; $j=3,4,5$) for the y series and P_{12} , P_{22} , P_{13} , P_{32} for the Padé series, are used. We also utilize the Bayesian evidence method to study which cosmographic approach performs the best. More details about the explicit cosmography expressions and Bayesian evidence are reported in Appendix A and B.

As a guideline, the Hubble parameter in the Λ CDM+ Ω_K model is introduced,

$$H(z) = H_0 \sqrt{\Omega_m(1+z)^3 + \Omega_K(1+z)^2 + (1 - \Omega_m - \Omega_K)}, \quad (14)$$

with corresponding cosmographic parameters being

$$q_0 = \frac{3}{2}\Omega_m + \Omega_K - 1, \quad (15)$$

$$j_0 = 1 - \Omega_K, \quad (16)$$

$$s_0 = 1 - \frac{9}{2}\Omega_m + \Omega_K^2 - \Omega_K(2 - \frac{3}{2}\Omega_m), \quad (17)$$

$$l_0 = 1 + 3\Omega_m + \frac{27}{2}\Omega_m^2 + \Omega_K^2 - \Omega_K(2 - 9\Omega_m), \quad (18)$$

where Ω_m represents the current matter density. In particular, when $\Omega_K = 0$ corresponds to the flat Λ CDM model, the terms containing Ω_K in the above equations will disappear.

In this paper, we use the newest Pantheon+ SNe Ia sample (Brout et al. 2022; Scolnic et al. 2022), the 14 latest BAO measurements (Alam et al. 2021), and the 32 OHD (Wu et al. 2023) obtained from cosmic chronometer method. More details about the data and fitting methods are reported in Appendix C.

3. CONSTRAINT RESULTS

We use CosmoMC (Lewis & Bridle 2002) together with a nested sampling plug-in, namely PolyChord (Handley et al. 2015a,b) which enables the computation of the Bayesian evidence, to study four cosmography models. With imposing uniform priors on the free parameters as listed in Table 1, we obtain the constraint results by numerical calculations, and summarize the mean and 68.3% confidence limits of cosmological parameters in Table 2. And, the likelihood distributions of y_1 , y_2 , y_3 and Padé approximations from the third order to the fifth order are shown in Figure 1–3, respectively. Furthermore, the logarithmic values of the Bayes factor $\ln B_{ij}$ for the Λ CDM+ Ω_K and the four cosmography models are given in Table 3 with the flat Λ CDM model as the reference model.

Table 1. The priors for the model parameters.

Parameters	Priors
H_0	[50, 90]
Ω_K	[-0.5, 0.5]
q_0	[-2, 0]
j_0	[-10, 10]
s_0	[-70, 70]
l_0	[-500, 500]
r_d	[130, 160]

Table 2. Constrained cosmographic parameters by the SNe Ia+OHD+BAO dataset under various expansion orders within the 1σ confidence level. Here, ‘-’ denotes there is no constraint result.

Model	H_0	Ω_K	q_0	j_0	s_0	l_0	r_d
Flat Λ CDM	68.30 ± 1.66	0	-0.53 ± 0.02	1	-0.41 ± 0.06	3.27 ± 0.14	145.70 ± 3.44
Λ CDM+ Ω_K	67.59 ± 1.66	0.095 ± 0.064	-0.48 ± 0.04	0.92 ± 0.07	-0.43 ± 0.06	3.07 ± 0.24	146.47 ± 3.46
$y_1^{(3)}$	68.27 ± 1.66	-0.123 ± 0.048	-0.40 ± 0.11	-0.7 ± 1.1	–	–	$144.99^{+3.14}_{-3.54}$
$y_1^{(4)}$	68.06 ± 1.66	-0.047 ± 0.080	$-0.54^{+0.13}_{-0.18}$	$2.3^{+3.0}_{-2.0}$	18.8 ± 26.6	–	145.52 ± 3.43
$y_1^{(5)}$	67.82 ± 1.71	$-0.013^{+0.084}_{-0.095}$	-0.42 ± 0.17	-0.7 ± 2.8	< -11.3	< -98	145.68 ± 3.56
$y_2^{(3)}$	69.07 ± 1.66	-0.219 ± 0.056	-0.45 ± 0.05	0.9 ± 0.1	–	–	143.44 ± 3.34
$y_2^{(4)}$	68.36 ± 1.69	-0.040 ± 0.086	-0.63 ± 0.08	$2.4^{+0.5}_{-0.6}$	$2.4^{+0.4}_{-1.1}$	–	144.96 ± 3.43
$y_2^{(5)}$	67.06 ± 1.68	0.029 ± 0.094	$-0.42^{+0.14}_{-0.11}$	$-0.2^{+1.0}_{-1.5}$	$-2.7^{+1.6}_{-2.6}$	71^{+30}_{-70}	147.68 ± 3.61
$y_3^{(3)}$	67.83 ± 1.71	0.005 ± 0.093	-0.451 ± 0.046	$1.0^{+0.1}_{-0.2}$	–	–	145.73 ± 3.53
$y_3^{(4)}$	67.56 ± 1.76	$0.025^{+0.087}_{-0.098}$	-0.54 ± 0.08	1.8 ± 0.6	$5.7^{+2.6}_{-3.9}$	–	146.44 ± 3.70
$y_3^{(5)}$	$67.08^{+1.64}_{-1.93}$	-0.001 ± 0.092	$-0.42^{+0.09}_{-0.13}$	$0.2^{+1.5}_{-1.9}$	4.1 ± 6.6	6^{+12}_{-27}	147.52 ± 3.79
P_{12}	67.54 ± 1.73	$0.032^{+0.088}_{-0.101}$	-0.38 ± 0.03	0.4 ± 0.1	–	–	$145.76^{+3.37}_{-3.75}$
P_{22}	67.51 ± 1.71	0.043 ± 0.083	$-0.57^{+0.10}_{-0.14}$	$3.2^{+1.8}_{-1.2}$	> 27.4	–	$146.36^{+3.36}_{-3.79}$
P_{13}	67.37 ± 1.75	$0.008^{+0.087}_{-0.099}$	-0.46 ± 0.05	0.8 ± 0.2	-0.6 ± 0.1	–	$146.74^{+3.45}_{-3.82}$
P_{32}	67.64 ± 1.77	0.038 ± 0.097	$-0.52^{+0.11}_{-0.13}$	$2.2^{+1.6}_{-1.0}$	$16.5^{+17.0}_{-8.7}$	> 159	146.01 ± 3.63

First, we focus on the Hubble constant H_0 and spatial curvature parameter Ω_K . From Table 2 we can see that the values of H_0 obtained from the four cosmographic approaches are consistent with the P18 value at 1σ confidence level (CL), and lower than the R22 value by $2.3\sim 3.0\sigma$. Meanwhile, they are in good agreement with that obtained from the flat Λ CDM and Λ CDM+ Ω_K models. Additionally, it is worth noting that under the Λ CDM+ Ω_K model and all cosmography models, a flat Universe is preferred by the present observations except for the $y_1^{(3)}$ and $y_2^{(3)}$ expansions in which a closed Universe is preferred at more than 2σ confidence level (CL). Meanwhile, from the $H_0 - \Omega_K$ plane in Figure 1–3, we can find that there is a visible anti-correlation between H_0 and Ω_K , indicating that a larger H_0 can be obtained from a smaller Ω_K , and in all the y approximations, the lower the expansion order, the smaller the constraint Ω_K .

Second, compared with $r_d = 147.05 \pm 0.3$ Mpc reported by Planck 2018, our constraints on r_d using all cosmographic approaches are in agreement with Planck 2018 within 1σ CL. Since the values of r_d are essentially the same including the mean value and the uncertainty in four cosmography models, from Table 2 and Figure 1–3, it can be concluded that the sound horizon r_d is not sensitive to the parameterization and truncation of the expansions. In addition, from the $H_0 - r_d$ contours, we can see that there is an obvious anti-correlation between r_d and H_0 . Therefore, if the expansion evolution of the Universe is determined, a smaller r_d would result in a larger H_0 , which can also be seen from Equation (C19).

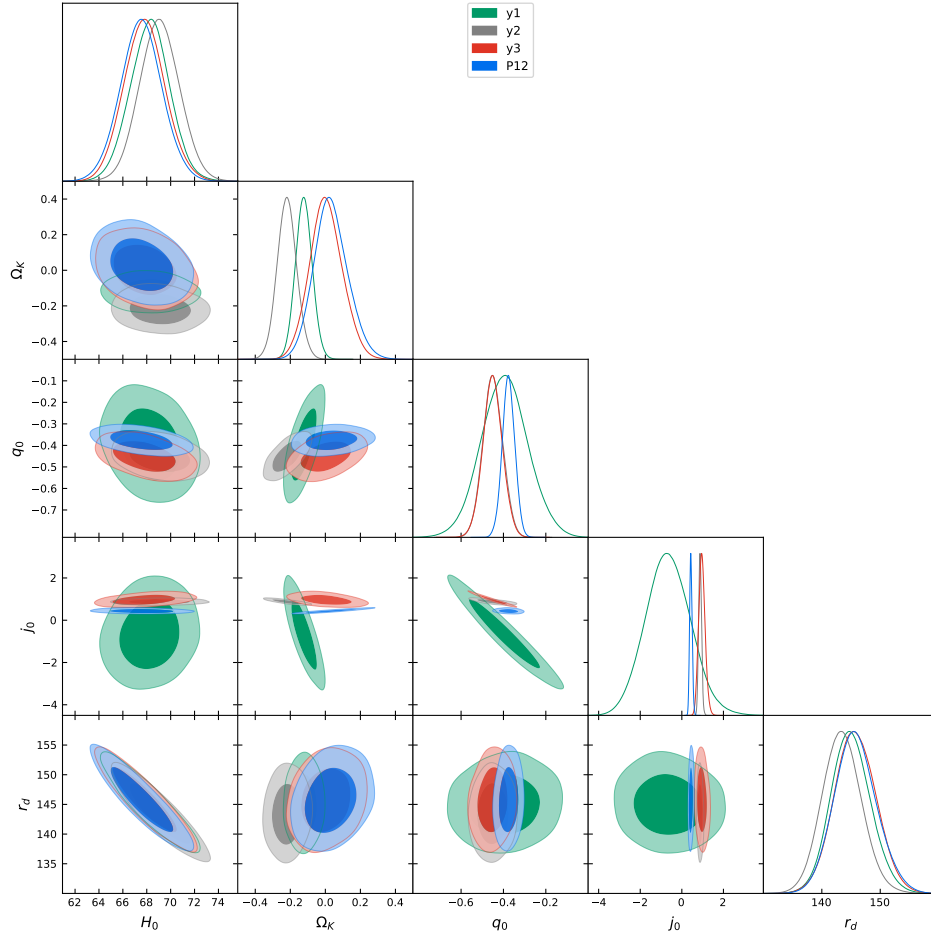


Figure 1. One-dimensional and two-dimensional marginalized distributions with 1σ and 2σ contours for the selected parameters under the third order.

Table 3. The values of $\ln B_{ij}$ computed for the selected cosmography model \mathcal{M}_i , where the reference scenario is the flat Λ CDM model (\mathcal{M}_j).

Model	$\ln B_{ij}$	Evidence against flat Λ CDM
Λ CDM+ Ω_K	-0.65 ± 0.16	Weak
$y_1^{(3)}$	-2.53 ± 0.16	Definite/positive
$y_1^{(4)}$	-2.66 ± 0.16	Definite/positive
$y_1^{(5)}$	-2.60 ± 0.17	Definite/positive
$y_2^{(3)}$	-7.62 ± 0.16	Very strong
$y_2^{(4)}$	-5.32 ± 0.17	Very strong
$y_2^{(5)}$	-5.26 ± 0.18	Very strong
$y_3^{(3)}$	-2.43 ± 0.16	Definite/positive
$y_3^{(4)}$	-3.45 ± 0.17	Strong
$y_3^{(5)}$	-4.40 ± 0.17	Strong
P_{12}	-3.70 ± 0.16	Strong
P_{22}	-1.92 ± 0.16	Definite/positive
P_{13}	-3.97 ± 0.17	Strong
P_{32}	-5.57 ± 0.18	Very Strong

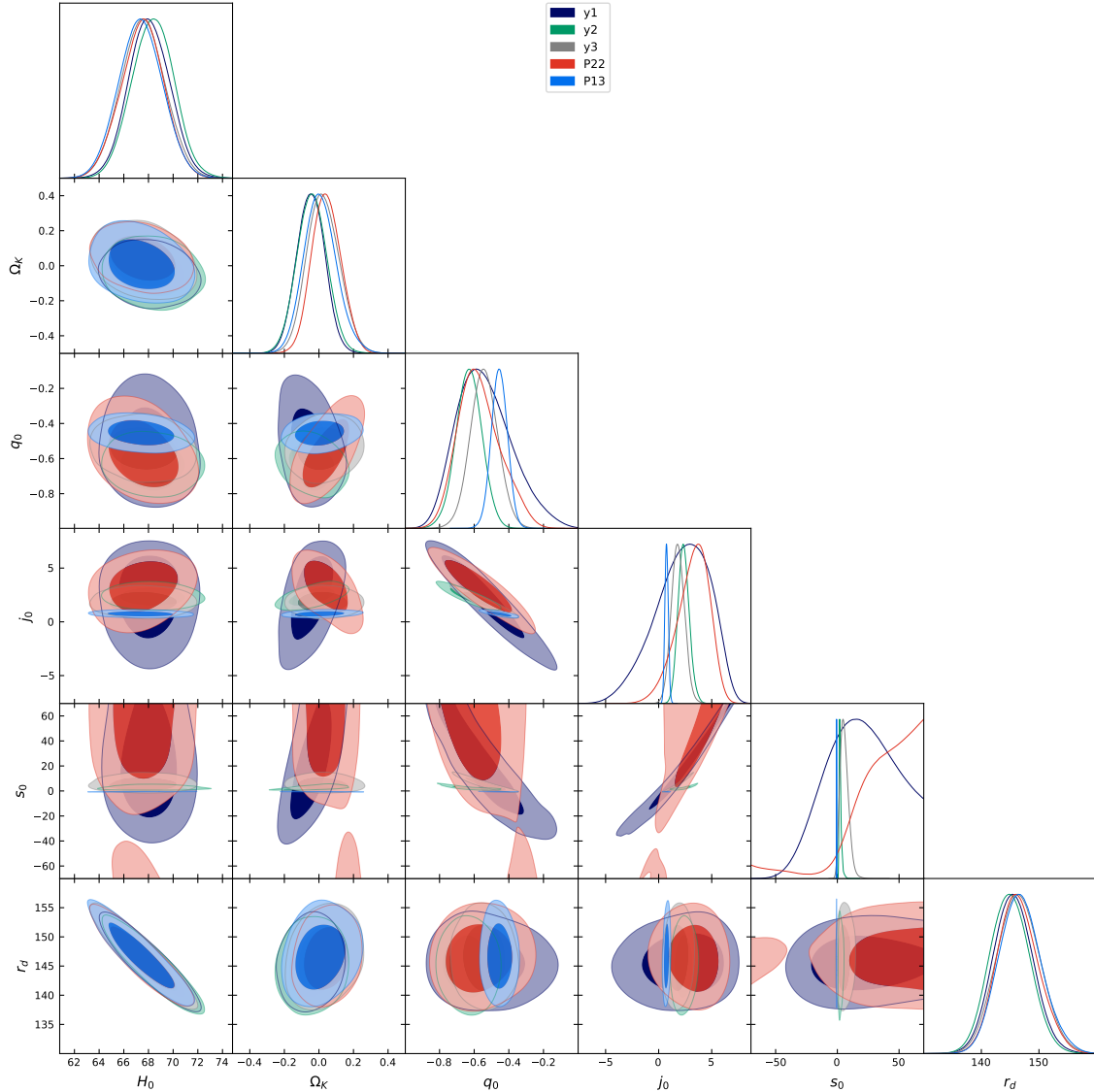


Figure 2. One-dimensional and two-dimensional marginalized distributions with 1σ and 2σ contours for the selected parameters under the fourth order.

Third, we analyze the constraints on the cosmological parameters q_0 , j_0 , s_0 and l_0 . From Table 2, it can be seen that the observations could provide a good constraint on the lower-order expansions, within which the values of q_0 and j_0 are basically consistent with that derived with the flat Λ CDM model, except the (1,2) order of Padé approximant. However, due to the complexity of high expansion orders and the insufficiency of high-redshift data, there are large uncertainties in the constraints of s_0 and l_0 by all the cosmography techniques. This suggests that new probes into the evolution of the Universe are needed to break the degeneracies of these parameters. Meanwhile, one can see from Table 2 that the uncertainties on the parameters of H_0 , Ω_K , and r_d remain roughly the same as one increases the expansion order, which is similar to the results obtained by Li et al. (2020). This is mainly because the degeneracy between the parameters of H_0 , Ω_K , and r_d , and the cosmographic parameters decreases with the expansion order increases as shown in Figures 1–3, and thus the constraint ability of observational data on the parameters of H_0 , Ω_K , and r_d is not substantially weakened with the increase of the number of model parameters.

Fourth, we apply the Bayesian evidences with the flat Λ CDM as the reference model to determine the most favored cosmography model for the joint datasets. From Table 3, one can see that all the $\ln B_{ij}$ values in this table are negative, indicating that the flat Λ CDM is the most preferred model by the observations, and the Λ CDM+ Ω_K model is also more favored than the four cosmography models. Furthermore, according to the Jeffreys scale list in Table 4, the

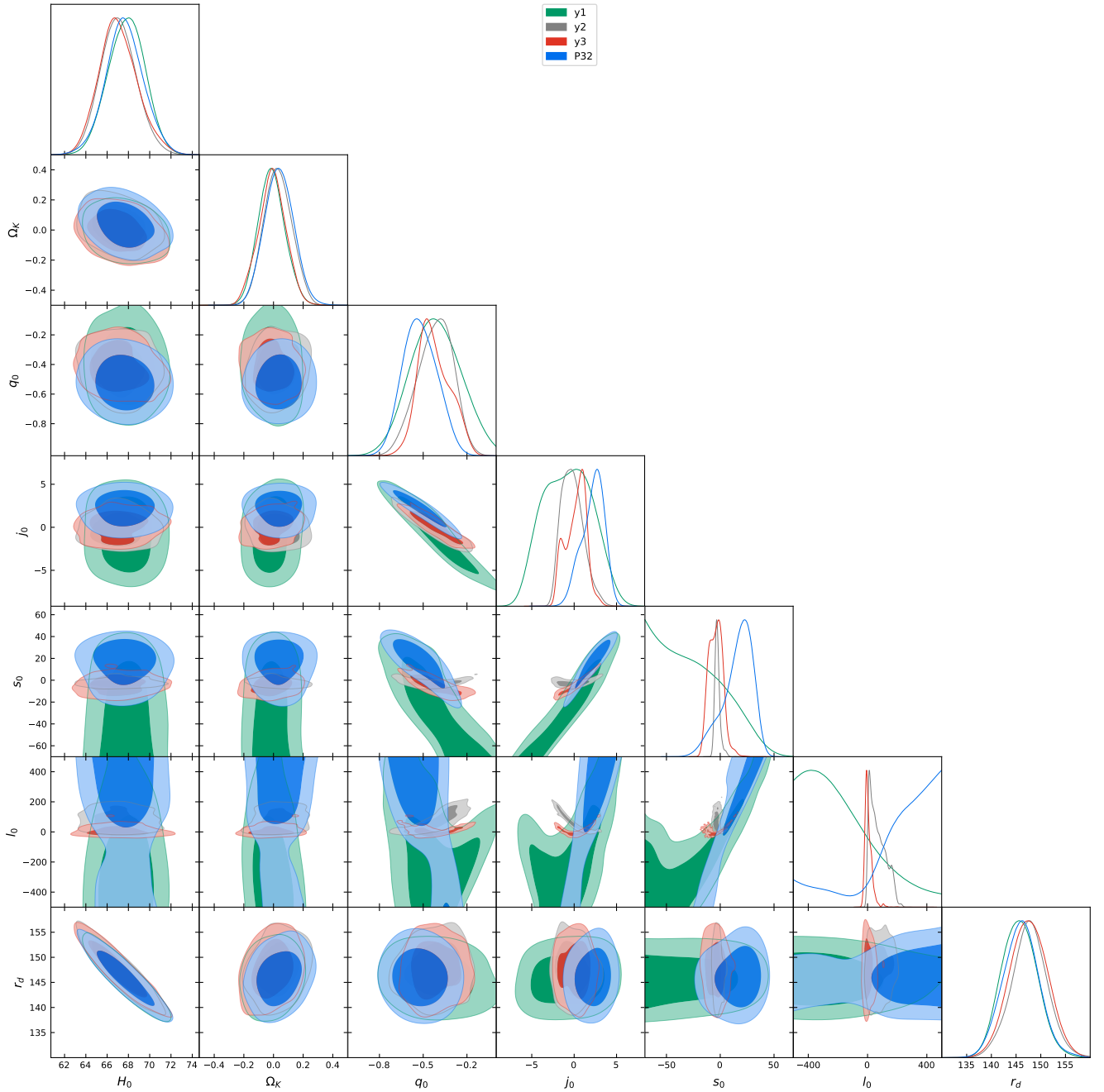


Figure 3. One-dimensional and two-dimensional marginalized distributions with 1σ and 2σ contours for the selected parameters under the fifth order.

$|\ln B_{ij}|$ values of five models, i.e. all expansions of y_1 , the third order of y_3 and the (2,2) order of Padé approximant, are smaller than 3, indicating that those models could fit the observations well. Especially, $y_1^{(3)}$, $y_3^{(3)}$ and P_{22} are the top three models that are most supported by the observations. Meanwhile, we find that all the y_2 expansions have the largest values of $|\ln B_{ij}|$ greater than 5, which means these kinds of expansions are strongly disfavored by the observational data, and can therefore be ruled out. In addition, we derive the evolutions of $H(z)$ within the $y_1^{(3)}$, $y_3^{(3)}$ and P_{22} models, and plot them combining the one obtained from the flat Λ CDM model for a comparison in Figure 4. One can see that the evolutions of $H(z)$ are consistent well with the prediction of flat Λ CDM model at the lower

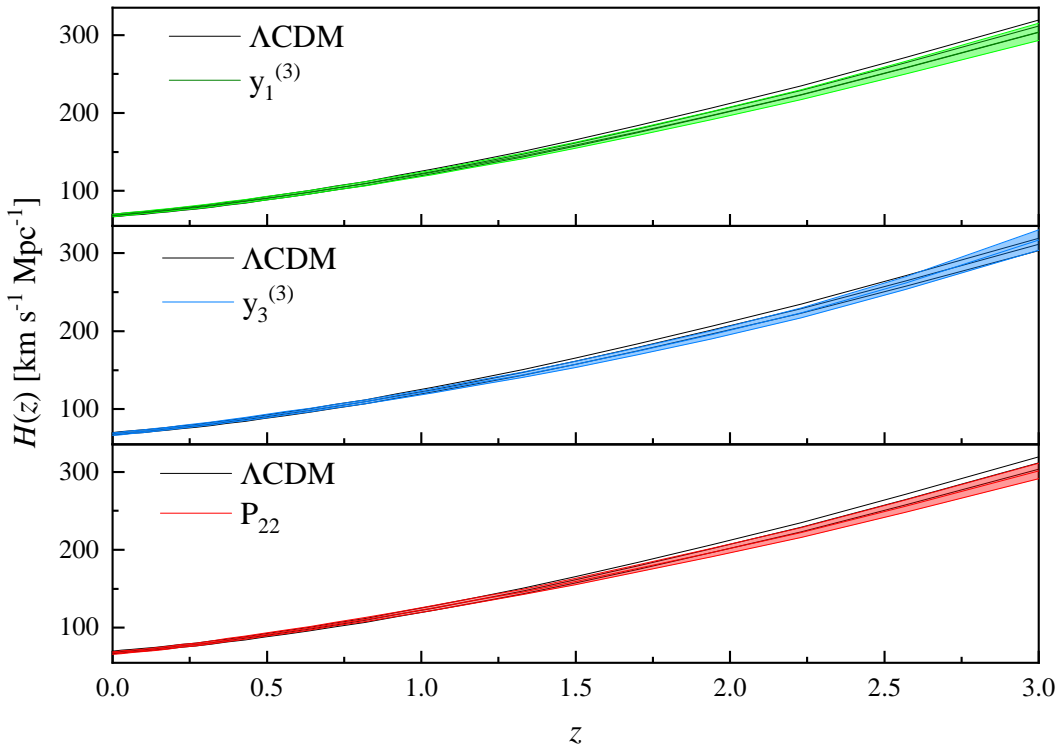


Figure 4. The reconstructed evolutions of $H(z)$ with the flat Λ CDM, $y_1^{(3)}$, $y_3^{(3)}$ and P_{22} models. The black lines show the center values and 1σ errors of $H(z)$ for flat Λ CDM model. The dark green, blue and red lines with light bands show the center values and 1σ errors of $H(z)$ for $y_1^{(3)}$, $y_3^{(3)}$ and P_{22} models, respectively.

redshift ($z < 1 \sim 1.5$). And although the evolutions of $H(z)$ from the cosmography models have some deviations from the flat Λ CDM model at the higher redshift, it is still in agreement with the flat Λ CDM model within 1σ CL.

Lastly, we compare our results with the previous works on the constraints of H_0 , Ω_K and r_d by model-independent methods. Adopting Taylor series in terms of y_1 and the Padé approximants along with the SNe Ia+OHD+BAO data, Li et al. (2020) showed that the tension level of H_0 has less than 2σ significance between different approximations and the local distance ladder determination while our constraint results show a tension of more than 2σ using the latest data. Furthermore, their constraint results on Ω_K preferred a closed Universe under all the approximations, whereas we find the newest datasets prefer a flat Universe with a higher precision. Therefore, the latest BAO measurements and Pantheon+ sample data can improve the accuracy of constraints on H_0 and Ω_K . Moreover, through Bayesian evidence, Li et al. (2020) found that the $y_1^{(3)}$ has weak evidence against Λ CDM+ Ω_K model and P_{22} has positive evidence, while our constraint results show that $y_3^{(3)}$ behaves the best in all series of y -variables with the updated BAO data and Pantheon+ SNe Ia sample. In addition, assuming a spatially flat Universe, Zhang & Huang (2021) reconstructed $H(z)$ in cubic expansion and polynomial expansion respectively, and constrained Hubble constant and sound horizon with the joint data of SNe Ia, BAO measurements, OHD, and GW data. And they found H_0 and r_d were consistent with the estimate derived from Planck 2018 data, which is similar to our constraint results. Likewise, Cao et al. (2022) combined 55 simulated SGLTD data and 1000 simulated GW data, and obtained high-precision constraint results $H_0 = 73.65 \pm 0.33 \text{ km s}^{-1}\text{Mpc}^{-1}$ and $\Omega_K = 0.008 \pm 0.038$. Although those results showed a strong constraint on H_0 comparing to our constraint results, those works use simulated data, whereas we use actual observational data.

4. CONCLUSION AND DISCUSSIONS

The Hubble tension problem can be relaxed to some extent by introducing Ω_K or any cosmological model that assumes a small r_d in the early Universe. In this paper, using the Pantheon+ sample of SNe Ia which significantly

enlarges the origin Pantheon sample size from 1048 to 1701, the 14 latest BAO measurements, and 32 OHD data, we constrain Hubble constant H_0 while leaving spatial curvature parameter Ω_K and sound horizon r_d completely free. In order to be model-independent, four cosmography approaches are taken, namely the Taylor expansions in terms of $y_1 = z/(1+z)$, $y_2 = \arctan z$, $y_3 = \ln(1+z)$ and the Padé approximants. We expand the transverse comoving distance and Hubble parameter with these four variables, and obtain the constraint results on H_0 , Ω_K , and r_d from the joint datasets. Then we adopt Bayesian evidence to determine which cosmography model gives the best approximation.

From the constraint results, we find that the newest Pantheon+ sample and updated BAO measurements could tighten the constraints on H_0 and Ω_K obviously. And the values of H_0 obtained from the four cosmography models are in good agreement with P18 and lower than R22 by $2.3\sim 3.0\sigma$. Meanwhile, a flat Universe is preferred by the observations under the Λ CDM+ Ω_K model and all cosmography approaches, except for $y_1^{(3)}$ and $y_2^{(3)}$. In addition, the constraints on r_d are consistent with the estimate derived from the Planck CMB data within 1σ under all expansions, suggesting that r_d is not sensitive to the approximations parameterizations. Furthermore, we find that there are anti-correlations between H_0 and Ω_K or H_0 and r_d , indicating smaller Ω_K or r_d would be helpful in alleviating the H_0 tension. Moreover, according to the Bayesian evidence, the Λ CDM is still the most favored model by the joint datasets. As for the cosmography models, the Padé approximant of order (2,2), the third order of y_3 and y_1 are the top three models that fit the datasets best, but the Taylor series in terms of y_2 are essentially excluded by cosmological observations.

As the final remarks, the release of H_0 tension in this paper is mainly caused by the increase in its uncertainty. If we take into account the full covariance of OHD (Moresco et al. 2020, 2022), the H_0 tension with R22 will decrease from $2.3\sim 3.0\sigma$ to $1.0\sim 1.9\sigma$ due to the further increased uncertainty. At the same time, the cosmographic parameters can not be constrained effectively when expanding up to high order. This suggests that more high-precision data and additional probes are needed to measure the cosmic expansion due to the degeneracy with Ω_K and cosmographic parameters. In the future, with the space-based GW detectors such as DECIGO (Seto et al. 2001; Kawamura et al. 2011), Taiji (Hu & Wu 2017), TianQin (TianQin collaboration 2016) and ET (Einstein Telescope) (Punturo et al. 2010) exploring more GW from BNS systems with EM counterparts, the constraints on H_0 and Ω_K will be more accurate and tight.

ACKNOWLEDGMENTS

We thank the anonymous reviewer for the insightful suggestions and comments. We also appreciate Professor Puxun Wu for the useful discussions. This work was supported by the National Natural Science Foundation of China under grants Nos. 12174227, 11974219, 11505004, and 11865018, the University Scientific Research Project of Anhui Province under grant No. 2022AH051634, and the Natural Science Foundation of Anhui Province under grant No. 1508085QA17.

REFERENCES

- Abbott, B. P., Abbott, R., Abbott, T. D., et al. 2017, *Nature*, 551, 85
- Abbott T. M. C., Abdalla, F. B. and Alarcon, A., et al. 2018, *PhRvD*, 98, 043526
- Alam, S., Ata, M., Bailey, S., et al. 2017, *MNRAS*, 470, 2617
- Alam, S., Aubert, M., Avila, S., et al. 2021, *PhRvD*, 103, 083533
- Anchordoqui, L. A. & Bergliaffa, S. E. P. 2019, *PhRvD*, 100, 123525
- Archidiacono, M., Gariazzo, S., Giunti, C., et al. 2020, *JCAP*, 2020, 029
- Aviles, A., Gruber, C., Luongo, O., et al. 2012, *PhRvD*, 86, 123516
- Bautista, J. E., Paviot, R., Vargas Magaña, M., et al. 2021, *MNRAS*, 500, 736
- Berghaus, K. V. & Karwal, T. 2020, *PhRvD*, 101, 083537
- Borghi, N., Moresco, M., & Cimatti, A. 2022, *ApJL*, 928, L4
- Brout, D., Scolnic, D., Popovic, B., et al. 2022, *ApJ*, 938, 110
- Buen-Abad, M. A., Schmaltz, M., Lesgourgues, J., et al. 2018, *JCAP*, 2018, 008
- Cai, R.-G., Guo, Z.-K., Wang, S.-J., et al. 2022, *PhRvD*, 106, 063519
- Cai, R.-G., Guo, Z.-K., Wang, S.-J., et al. 2022, *PhRvD*, 105, L021301
- Caldwell, R. R. & Kamionkowski, M. 2004, *JCAP*, 2004, 009

- Cao, M.-D., Zheng, J., Qi, J.-Z., et al. 2022, *ApJ*, 934, 108
- Capozziello, S., Carloni, S., & Troisi, A. 2003, [arxiv:astro-ph/0303041](https://arxiv.org/abs/astro-ph/0303041)
- Capozziello, S., De Laurentis, M., Luongo, O., et al. 2013, *Galax*, 1, 216
- Capozziello, S., D’Agostino, R., & Luongo, O. 2018, *MNRAS*, 476, 3924
- Capozziello, S., D’Agostino, R., & Luongo, O. 2019, *IJMPD*, 28, 1930016
- Capozziello, S., D’Agostino, R., & Luongo, O. 2020, *MNRAS*, 494, 2576
- Carneiro, S., de Holanda, P. C., Pigozzo, C., et al. 2019, *PhRvD*, 100, 023505
- Cattoën, C. & Visser, M. 2007, *CQGra*, 24, 5985
- Chiba, T. & Nakamura, T. 1998, *PThPh*, 100, 1077
- Colgáin, E. Ó., Sheikh-Jabbari, M. M., & Yin, L. 2021, *PhRvD*104, 023510
- Conley, A., Guy, J., Sullivan, M., et al. 2011, *ApJS*, 192, 1
- D’Eramo, F., Di Valentino, E., Giarè, W., et al. 2022, *JCAP*, 09, 022
- de Mattia, A., Ruhlmann-Kleider, V., Raichoor, A., et al. 2021, *MNRAS*, 501, 5616
- Di Valentino, E., Melchiorri, A., & Silk, J. 2016, *PhLB*, 761, 242
- Di Valentino, E., Melchiorri, A., Fantaye, Y., et al. 2018, *PhRvD*, 98, 063508
- Di Valentino, E., Melchiorri, A., & Silk, J. 2020, *NatAs*, 4, 196
- Di Valentino, E., Melchiorri, A., & Silk, J. 2021, *ApJL*, 908, L9
- Dossett, J. N. & Ishak, M. 2012, *PhRvD*, 86, 103008
- du Mas des Bourboux, H., Rich, J., Font-Ribera, A., et al. 2020, *ApJ*, 901, 153
- Dunsby, P. K. S. & Luongo, O. 2016, *IJGMM*, 13, 1630002-606
- Farrugia, C. R., Sultana, J., & Mifsud, J. 2021, *PhRvD*, 104, 123503
- Feeney, S. M., Mortlock, D. J., & Dalmaso, N. 2018, *MNRAS*, 476, 3861
- Freedman, W. L., Madore, B. F., Hoyt, T., et al. 2020, *ApJ*, 891, 57
- Freedman, W. L. 2017, *NatAs*, 1, 0169
- Gil-Marín, H., Bautista, J. E., Paviot, R., et al. 2020, *MNRAS*, 498, 2492
- Gruber, C. & Luongo, O. 2014, *PhRvD*, 89, 103506
- Handley, W. 2021, *PhRvD*, 103, L041301
- Handley, W.-J., Hobson, M.-P., & Lasenby, A.-N. 2015, *MNRAS*, 450, L61
- Handley, W.-J., Hobson, M.-P., & Lasenby, A.-N. 2015, *MNRAS*, 453, 4384
- Hogg, D. W. 1999, [arxiv:astro-ph/9905116](https://arxiv.org/abs/astro-ph/9905116).
- Hou, J., Sánchez, A.-G., Ross, A.-J., et al. 2021, *MNRAS*, 500, 1201
- Hu, J.-P. & Wang, F.-Y. 2022, *MNRAS*, 517, 576.
- Hu, W.-R. & Wu Y.-L. 2017, *Natl. Sci. Rev.*, 4, 685
- Huang, Q.-G. & Wang, K. 2016, *EPJC*, 76, 506
- Jalilvand, F. & Mehrabi, A. 2022, *EPJP*, 137, 1341
- Jedamzik, K., Pogosian, L., & Zhao, G.-B. 2021, *CmPhy*, 4, 123
- Karwal, T. & Kamionkowski, M. 2016, *PhRvD*, 94, 103523
- Kass R. E., Raftery A. E., 1995, *J. Am. Statist. Assoc.*, 90, 773
- Kawamura, S., Ando, M., Seto, N., et al. 2011, *CQGra*, 28, 094011
- Kessler, R. & Scolnic, D. 2017, *ApJ*, 836, 56
- Koussour, M., El Bourakadi, K., Shekh, S. H., et al. 2022, *AnPhy*, 445, 169092
- Kumar, S. & Nunes, R. C. 2016, *PhRvD*, 94, 123511
- Lewis, A. & Bridle, S. 2002, *PhRvD*, 66, 103511
- Li, E.-K., Du, M., & Xu, L. 2020, *MNRAS*, 491, 4960
- Liu, T., Cao, S., Biesiada, M., et al. 2022, *ApJ*, 939, 37
- Miao, H. & Huang, Z. 2018, *ApJ*, 868, 20
- Moresco, M., Cimatti, A., Jimenez, R., et al. 2012, *JCAP*, 2012, 006
- Moresco, M., Pozzetti, L., Cimatti, A., et al. 2016, *JCAP*, 2016, 014
- Moresco, M. 2015, *MNRAS*, 450, L16
- Moresco, M., Jimenez, R., Verde, L., et al. 2020, *ApJ*, 898, 82
- Moresco, M., Amati, L., Amendola, L., et al. 2022, *LRR*, 25, 6
- Neveux, R., Burtin, E., de Mattia, A., et al. 2020, *MNRAS*, 499, 210
- Niedermann, F. & Sloth, M. S. 2020, *PhRvD*, 102, 063527
- Nunes, R. C. 2018, *JCAP*, 2018, 052
- Pandey, K. L., Karwal, T., & Das, S. 2020, *JCAP*, 2020, 026
- Planck Collaboration, Aghanim, N., Akrami, Y., et al. 2020, *A&A*, 641, A6
- Pogosian, L., Zhao, G.-B., & Jedamzik, K., 2020, 2020, *ApJL*904, L17
- Popovic, B., Brout, D., Kessler, R., et al. 2021, *ApJ*, 913, 49
- Poulin, V., Smith, T. L., Karwal, T., et al. 2019, *PhRvL*, 122, 221301
- Punturo, M., Abernathy, M., Acernese, F., et al. 2010, *CQGra*, 27, 194002
- Ratsimbazafy, A. L., Loubser, S. I., Crawford, S. M., et al. 2017, *MNRAS*, 467, 3239
- Riess, A. G., Casertano, S., Yuan, W., Macri, L. M., and Scolnic, D., 2019, *ApJ*, 876, 85

- Riess, A. G., Yuan, W., Macri, L. M., et al. 2022, *ApJL*, 934, L7
- Ross, A. J., Samushia, L., Howlett, C., et al. 2015, *MNRAS*, 449, 835
- Scolnic, D., Brout, D., Carr, A., et al. 2022, *ApJ*, 938, 113
- Semiz, İ. & Kazım Çamlıbel, A. 2015, *JCAP*, 2015, 038
- Seto, N., Kawamura, S., & Nakamura, T. 2001, *PhRvL*, 87, 221103
- Shafieloo, A. 2012, *JCAP*, 2012, 002
- Simon, J., Verde, L., & Jimenez, R. 2005, *PhRvD*, 71, 123001
- Stern, D., Jimenez, R., Verde, L., et al. 2010, *JCAP*, 2010, 008
- Sultana, J., Yennapureddy, M. K., Melia, F., et al. 2022, *MNRAS*, 514, 5827
- Suyu, S. H., Bonvin, V., Courbin, F., et al. 2017, *MNRAS*, 468, 2590
- Luo, J., Chen, L.-S., Duan, H.-Z., et al. 2016, *CQGra*, 33, 035010
- Trotta, R. 2008, *ConPh*, 49, 71
- Vagnozzi, S., Loeb, A., & Moresco, M. 2021, *ApJ*, 908, 84
- Visser, M. 2004, *CQGra*, 21, 2603
- Visser, M. 2005, *GReGr*, 37, 1541
- Visser, M. 2015, *CQGra*, 32, 135007
- Wang, G.-J., Ma, X.-J., & Xia, J.-Q. 2021, *MNRAS*, 501, 5714
- Wei, H., Yan, X.-P., & Zhou, Y.-N. 2014, *JCAP*, 2014, 045
- Wojtak, R. & Agnello, A. 2019, *MNRAS*, 486, 5046
- Wu, P.-J., Qi, J.-Z., & Zhang, X. 2023, *ChPhC*, 47, 055106
- Xu, L. & Huang, Q.-G. 2018, *SCPMA*, 61, 39521
- Yang, W., Pan, S., Di Valentino, E., et al. 2019, *PhRvD*, 99, 043543
- Yang, T., Banerjee, A., & Ó Colgáin, E. 2020, *PhRvD*, 102, 123532
- Yang, W., Giarè, W., Pan, S., et al. 2023, *PhRvD*107, 063509
- Yin, Z.-Y., Wei, H. 2019, *EPJC*, 79, 698
- Zhao, G.-B., Raveri, M., Pogosian, L., et al. 2017, *NatAs*, 1, 627
- Zhang, C., Zhang, H., Yuan, S., et al. 2014, *RAA*, 14, 1221-1233
- Zhang, M.-J., Li, H. & Xia, J.-Q. 2017, *EPJC*, 77, 434
- Zhang, X. & Huang, Q.-G. 2021, *PhRvD*, 103, 043513

APPENDIX

A. COSMOGRAPHIC EXPANSIONS

In this section, all the cosmographic expansions up to the fifth order which we adopted in this study are reported.

(i) the transverse comoving distance within the y_1 -variable model:

$$\begin{aligned}
D_M(y_1) = & \frac{c}{H_0} \left[y_1 + \frac{1}{2}(1 - q_0)y_1^2 + \frac{1}{6}(2 - j_0 - 2q_0 + 3q_0^2 + \Omega_K)y_1^3 \right. \\
& + \frac{1}{24}(6 - 3j_0 - 6q_0 + 10j_0q_0 + 9q_0^2 - 15q_0^3 + s_0 + 6\Omega_K - 6q_0\Omega_K)y_1^4 \\
& + \frac{1}{120}(24 - 12j_0 + 10j_0^2 - l_0 - 24q_0 + 40j_0q_0 + 36q_0^2 - 105j_0q_0^2 - 60q_0^3 \\
& \left. + 105q_0^4 + 4s_0 - 15q_0s_0 + 35\Omega_K - 10j_0\Omega_K - 50q_0\Omega_K + 45q_0^2\Omega_K + \Omega_K^2)y_1^5 \right]
\end{aligned} \tag{A1}$$

(ii) the transverse comoving distance within the y_2 -variable model:

$$\begin{aligned}
D_M(y_2) = & \frac{c}{H_0} \left[y_2 + \frac{1}{2}(-1 - q_0)y_2^2 + \frac{1}{6}(4 - j_0 + 4q_0 + 3q_0^2 + \Omega_K)y_2^3 \right. \\
& + \frac{1}{24}(-14 + 9j_0 - 26q_0 + 10j_0q_0 - 27q_0^2 - 15q_0^3 + s_0 - 6\Omega_K - 6q_0\Omega_K)y_2^4 \\
& + \frac{1}{120}(80 - 92j_0 + 10j_0^2 - l_0 + 176q_0 - 160j_0q_0 + 276q_0^2 - 105j_0q_0^2 + 240q_0^3 \\
& \left. + 105q_0^4 - 16s_0 - 15q_0s_0 + 55\Omega_K - 10j_0\Omega_K + 70q_0\Omega_K + 45q_0^2\Omega_K + \Omega_K^2)y_2^5 \right]
\end{aligned} \tag{A2}$$

(iii) the transverse comoving distance within the y_3 -variable model:

$$\begin{aligned}
D_M(y_3) = & \frac{c}{H_0} \left[y_3 - \frac{1}{2}q_0y_3^2 + \frac{1}{6}(-j_0 + q_0 + 3q_0^2 + \Omega_K)y_3^3 \right. \\
& + \frac{1}{24}(3j_0 - q_0 + 10j_0q_0 - 9q_0^2 - 15q_0^3 + s_0 - 6q_0\Omega_K)y_3^4 \\
& + \frac{1}{120}(-7j_0 + 10j_0^2 - l_0 + q_0 - 60j_0q_0 + 21q_0^2 - 105j_0q_0^2 + 90q_0^3 \\
& \left. + 105q_0^4 - 6s_0 - 15q_0s_0 - 10j_0\Omega_K + 10q_0\Omega_K + 45q_0^2\Omega_K + \Omega_K^2)y_3^5 \right]
\end{aligned} \tag{A3}$$

(iv) P_{12} approximation of the transverse comoving distance:

$$\begin{aligned}
P_{12} = & \frac{c}{H_0} \frac{z}{1 + b_1z + b_2z^2} \\
b_1 = & \frac{1}{2}(1 + q_0) \\
b_2 = & \frac{1}{12}(-1 + 2j_0 - 2q_0 - 3q_0^2 - 2\Omega_K)
\end{aligned} \tag{A4}$$

(v) P_{13} approximation of the transverse comoving distance:

$$\begin{aligned}
P_{13} = & \frac{c}{H_0} \frac{z}{1 + b_1z + b_2z^2 + b_3z^3} \\
b_1 = & \frac{1}{2}(1 + q_0) \\
b_2 = & \frac{1}{12}(-1 + 2j_0 - 2q_0 - 3q_0^2 - 2\Omega_K) \\
b_3 = & \frac{1}{24}(1 - 5j_0 + 3q_0 - 6j_0q_0 + 8q_0^2 + 6q_0^3 - s_0 + 2\Omega_K + 2q_0\Omega_K)
\end{aligned} \tag{A5}$$

(vi) P_{22} approximation of the transverse comoving distance:

$$P_{22} = \frac{c}{H_0} \frac{z + \frac{1}{2} \frac{a_2}{c_1} z^2}{1 + \frac{1}{2} \frac{b_1}{c_1} z + \frac{1}{12} \frac{b_2}{c_1} z^2}$$

$$\begin{aligned} a_2 &= -1 + 5j_0 - 3q_0 + 6j_0q_0 - 8q_0^2 - 6q_0^3 + s_0 - 2\Omega_K - 2q_0\Omega_K \\ b_1 &= -2 + 7j_0 - 6q_0 + 8j_0q_0 - 13q_0^2 - 9q_0^3 + s_0 - 4\Omega_K - 4q_0\Omega_K \\ b_2 &= 2 - 11j_0 - 4j_0^2 + 8q_0 - 25j_0q_0 + 23q_0^2 - 6j_0q_0^2 + 30q_0^3 - 3s_0 \\ &\quad - 3q_0s_0 + 2\Omega_K + 8j_0\Omega_K + 4q_0\Omega_K - 6q_0^2\Omega_K - 4\Omega_K^2 \\ c_1 &= -1 + 2j_0 - 2q_0 - 3q_0^2 - 2\Omega_K \end{aligned} \tag{A6}$$

(vii) P_{32} approximation of the transverse comoving distance:

$$P_{32} = \frac{c}{H_0} \frac{z + \frac{1}{10} \frac{a_2}{c_1} z^2 + \frac{1}{60} \frac{a_3}{c_1} z^3}{1 + \frac{1}{5} \frac{b_1}{c_1} z + \frac{1}{20} \frac{b_2}{c_1} z^2}$$

$$\begin{aligned} a_2 &= 14 - 137j_0 - 10j_0^2 - 6l_0 + 70q_0 - 472j_0q_0 - 20j_0^2q_0 - 6l_0q_0 + 277q_0^2 - 495j_0q_0^2 \\ &\quad + 551q_0^3 - 150j_0q_0^3 + 465q_0^4 + 135q_0^5 - 61s_0 - 10j_0s_0 - 116q_0s_0 - 45q_0^2s_0 + 20\Omega_K \\ &\quad + 50j_0\Omega_K + 60q_0\Omega_K + 60j_0q_0\Omega_K + 10q_0^2\Omega_K - 30q_0^3\Omega_K + 10s_0\Omega_K - 34\Omega_K^2 - 34q_0\Omega_K^2 \\ a_3 &= 4 - 60j_0 + 9j_0^2 - 80j_0^3 - 6l_0 + 12j_0l_0 + 24q_0 - 276j_0q_0 - 12l_0q_0 + 120q_0^2 - 468j_0q_0^2 \\ &\quad + 180j_0^2q_0^2 - 18l_0q_0^2 + 320q_0^3 - 330j_0q_0^3 + 423q_0^4 - 270j_0q_0^4 + 270q_0^5 + 135q_0^6 - 36s_0 \\ &\quad - 18j_0s_0 - 102q_0s_0 - 60j_0q_0s_0 - 78q_0^2s_0 - 15s_0^2 + 18\Omega_K - 144j_0\Omega_K + 120j_0^2\Omega_K \\ &\quad - 12l_0\Omega_K + 72q_0\Omega_K - 360j_0q_0\Omega_K + 252q_0^2\Omega_K - 420j_0q_0^2\Omega_K + 360q_0^3\Omega_K + 270q_0^4\Omega_K \\ &\quad - 72s_0\Omega_K - 60q_0s_0\Omega_K + 6\Omega_K^2 - 12j_0\Omega_K^2 + 12q_0\Omega_K^2 + 18q_0^2\Omega_K^2 - 28\Omega_K^3 \\ b_1 &= 12 - 96j_0 - 15j_0^2 - 3l_0 + 60q_0 - 326j_0q_0 - 20j_0^2q_0 - 3l_0q_0 + 216q_0^2 - 325j_0q_0^2 \\ &\quad + 408q_0^3 - 90j_0q_0^3 + 330q_0^4 + 90q_0^5 - 38s_0 - 5j_0s_0 - 73q_0s_0 - 30q_0^2s_0 + 15\Omega_K \\ &\quad + 45j_0\Omega_K + 45q_0\Omega_K + 50j_0q_0\Omega_K - 30q_0^3\Omega_K + 5s_0\Omega_K - 27\Omega_K^2 - 27q_0\Omega_K^2 \\ b_2 &= 12 - 132j_0 - 37j_0^2 - 40j_0^3 - 8l_0 + 4j_0l_0 + 72q_0 - 0 - 596j_0q_0 - 100j_0^2q_0 \\ &\quad - 16l_0q_0 + 312q_0^2 - 898j_0q_0^2 + 40j_0^2q_0^2 - 12l_0q_0^2 + 768q_0^3 - 510j_0q_0^3 + 927q_0^4 \\ &\quad - 180j_0q_0^4 + 510q_0^5 + 135q_0^6 - 68s_0 - 26j_0s_0 - 196q_0s_0 - 40j_0q_0s_0 - 162q_0^2s_0 \\ &\quad - 30q_0^3s_0 - 5s_0^2 + 16\Omega_K^2 + 32j_0\Omega_K + 80j_0^2\Omega_K - 4l_0\Omega_K + 64q_0\Omega_K + 60j_0q_0\Omega_K \\ &\quad + 64q_0^2\Omega_K - 120j_0q_0^2\Omega_K + 60q_0^4\Omega_K - 4s_0\Omega_K - 32\Omega_K^2 - 44j_0\Omega_K^2 - 64q_0\Omega_K^2 + 12q_0^2\Omega_K^2 + 4\Omega_K^3 \\ c_1 &= 2 - 11j_0 - 4j_0^2 + 8q_0 - 25j_0q_0 + 23q_0^2 - 6j_0q_0^2 + 30q_0^3 + 9q_0^4 - 3s_0 - 3q_0s_0 \\ &\quad + 2\Omega_K + 8j_0\Omega_K + 4q_0\Omega_K - 6q_0^2\Omega_K - 4\Omega_K^2 \end{aligned} \tag{A7}$$

B. BAYESIAN EVIDENCE METHOD

Bayesian evidence provides a statistical way to evaluate the performances of the cosmography models. For a given model \mathcal{M} with parameter space θ and specific observational data d , the Bayesian evidence E is defined as

$$E = p(d|\mathcal{M}) = \int p(d|\theta, \mathcal{M})\pi(\theta|\mathcal{M})d\theta, \tag{B8}$$

where $\pi(\theta|\mathcal{M})$ is the prior of θ in model \mathcal{M} , and $p(d|\theta, \mathcal{M})$ is the likelihood. Then, for the two models \mathcal{M}_i and \mathcal{M}_j , combing the Bayes theorem, the posterior probability is

$$\frac{p(\mathcal{M}_i|d)}{p(\mathcal{M}_j|d)} = \frac{p(d|\mathcal{M}_i)}{p(d|\mathcal{M}_j)} \frac{\pi(\mathcal{M}_i)}{\pi(\mathcal{M}_j)}. \tag{B9}$$

Table 4. Revised Jeffreys scale quantifying the observational viability of any model \mathcal{M}_i compared with some reference model \mathcal{M}_j .

$\ln B_{ij}$	Strength of evidence for model \mathcal{M}_i
$0 < \ln B_{ij} < 1$	Weak
$1 < \ln B_{ij} < 3$	Definite/positive
$3 < \ln B_{ij} < 5$	Strong
$ \ln B_{ij} > 5$	Very strong

The ratio between posterior probabilities leads to the definition of the Bayes factor B_{ij} , which is written in a logarithmic scale as

$$\ln B_{ij} = \ln \frac{p(d|\mathcal{M}_i)}{p(d|\mathcal{M}_j)} = \ln p(d|\mathcal{M}_i) - \ln p(d|\mathcal{M}_j). \quad (\text{B10})$$

Then, one can determine the strength of the preference for one of the competing models over the other by means of the Jeffreys scale listed in Table 4 (Trotta 2008; Kass et al. 1995).

C. DATA AND FITTING METHODS

In this section, we introduce the observational data and fitting methods used in our work.

C.1. SNe Ia

As the standard candle, SNe Ia is widely used to measure the cosmological luminosity distance. In our analysis, the largest SNe Ia sample Pantheon+ is used. Pantheon+ consists of 1701 light curves of 1550 spectroscopically confirmed SNe Ia across 18 different surveys, and covers the redshift range $z \in [0.00122, 2.26137]$. The observed distance modulus of each SNe Ia in this sample is defined as

$$\mu_{\text{obs}} = m_{\text{B}}^* + \alpha X_1 - \beta \mathcal{C} - M_{\text{B}} - \delta_{\text{bias}} + \delta_{\text{host}}, \quad (\text{C11})$$

Here, m_{B}^* is the observed peak magnitude in rest frame B-band, X_1 is the time stretching of the light-curve, \mathcal{C} is the SNe Ia color at maximum brightness, M_{B} is the absolute magnitude, α , β are two nuisance parameters, which should be fitted simultaneously with the cosmological parameters. And δ_{bias} is a correction term to account for selection biases, δ_{host} is the luminosity correction for residual correlations between the standardized brightness of an SNe Ia and the host-galaxy mass. In order to avoid the dependence of the nuisance parameters on the cosmological model, Kessler & Scolnic (2017) proposed a new method called BEAMS with bias corrections (BBC) to calibrate the SNe Ia, and the corrected apparent magnitude $m_{\text{B,corr}}^* = m_{\text{B}}^* + \alpha X_1 - \beta \mathcal{C} - M_{\text{B}} - \delta_{\text{bias}} + \delta_{\text{host}}$ for all the SNe Ia is reported in Popovic et al. (2021). Then the observed distance modulus is rewritten as

$$\mu_{\text{obs}} = m_{\text{B,corr}}^* - M_{\text{B}}, \quad (\text{C12})$$

On the other hand, introducing the Hubble-free luminosity $d_{\text{L}}(z) = H_0 D_{\text{L}}(z)$, the theoretical value of distance modulus can be derived from

$$\mu_{\text{th}}(z) = 5 \log(d_{\text{L}}) + \mu_0, \quad (\text{C13})$$

where $\mu_0 = 42.38 - 5 \log h$ with $h = H_0/100 \text{ km s}^{-1} \text{ Mpc}^{-1}$. Therefore, the χ^2 function for the Pantheon+ SNe Ia data can be written as

$$\chi_{\text{SNIa}}^2 \equiv \Delta \boldsymbol{\mu}^{\text{T}} \cdot \mathbf{Cov}^{-1} \cdot \Delta \boldsymbol{\mu}, \quad (\text{C14})$$

where $\Delta \mu_i = m_{\text{B,corr}}^* - 5 \log d_{\text{L}}(z) - \mathcal{N}$, and \mathbf{Cov} is the covariance matrix, respectively. Here, $\mathcal{N} = M_{\text{B}} + \mu_0$, which can be marginalized over analytically with the method proposed in Conley et al. (2011). Finally, the χ^2 function is rewritten as

$$\chi_{\text{SNIa,marg}}^2 = a - \frac{b^2}{f} + \ln \frac{f}{2\pi} \quad (\text{C15})$$

where $a \equiv \Delta \mathbf{m}^T \cdot \mathbf{Cov}^{-1} \cdot \Delta \mathbf{m}$, $b \equiv \Delta \mathbf{m}^T \cdot \mathbf{Cov}^{-1} \cdot \mathbf{1}$, $f \equiv \mathbf{1}^T \cdot \mathbf{Cov}^{-1} \cdot \mathbf{1}$. Here, it should be pointed out that since that the sensitivity of peculiar velocities of SNe Ia is very large at $z < 0.01$ and thus the Hubble residual bias can not be negligible, the SNe Ia data with $z > 0.01$ is only used instead of the full sample, in our analysis. We refer the reader to the Ref. (Brout et al. (2022)) for further details on this issue.

C.2. BAO

BAO data have provided another way to probe the expansion rate and the large-scale properties of the Universe, which give information about the imprint in the primordial plasma. The BAO data used in this paper include the measurements from the Sloan Digital Sky Survey Data Release 7 (SDSS DR7) main galaxy sample (MGS) (Ross et al. 2015), the SDSS-III BOSS DR12 galaxy sample (Alam et al. 2017), the SDSS-IV eBOSS DR16 LRG sample (Gil-Marín et al. 2020), the SDSS-IV eBOSS DR16 ELG sample (de Mattia et al. 2021), the SDSS-VI eBOSS DR16 quasars (QSO) sample (Neveux et al. 2020), the eBOSS DR16 auto-correlations and cross-correlations of the Ly α absorption and quasars (du Mas des Bourboux et al. 2020). We summarize these data in Table 5.

We note that the likelihoods of MGS data, DR16 Ly α -Ly α and DR16 Ly α -QSO data used in this work cannot be well approximated by a Gaussian. Thus, their full likelihoods are used. The 4×4 covariance matrix for DR12 LRG data from Gil-Marín et al. (2020) is

$$\begin{pmatrix} 0.0286052 & -0.04939281 & 0.01489688 & -0.01387079 \\ -0.04939281 & 0.5307187 & -0.02423513 & 0.1767087 \\ 0.01489688 & -0.02423513 & 0.04147534 & -0.04873962 \\ -0.01387079 & 0.1767087 & -0.04873962 & 0.3268589 \end{pmatrix} \quad (\text{C16})$$

The 2×2 covariance matrix for DR16 LRG data from Bautista et al. (2021) is

$$\begin{pmatrix} 0.1076634008565565 & -0.05831820341302727 \\ -0.05831820341302727 & 0.2838176386340292 \end{pmatrix} \quad (\text{C17})$$

The 2×2 covariance matrix for DR16 QSO data from Hou et al. (2021) is

$$\begin{pmatrix} 0.63731604 & 0.1706891 \\ 0.1706891 & 0.30468415 \end{pmatrix} \quad (\text{C18})$$

In Table 5, the observable $D_V \equiv [czD_M(z)/H(z)]^{1/3}$ is the volume average distance and $D_H \equiv c/H(z)$ is the Hubble distance. The parameter r_d is comoving sound horizon at the end of radiation drag epoch z_d , shortly after recombination, when baryons decouple from the photons,

$$r_d = \int_{z_d}^{\infty} \frac{c_s(z)}{H(z)} dz, \quad (\text{C19})$$

where $c_s(z)$ is the sound speed of the photon-baryon fluid. In this paper, the parameter r_d is treated as a free parameter.

Finally, the BAO data are combined into a χ^2 -statistic

$$\begin{aligned} \chi_{\text{BAO}}^2 = & \chi_{\text{MGS}}^2 + \chi_{\text{DR12LRG}}^2 + \chi_{\text{DR16LRG}}^2 + \chi_{\text{DR16ELG}}^2 \\ & + \chi_{\text{DR16QSO}}^2 + \chi_{\text{DR16Ly}\alpha\text{-Ly}\alpha}^2 + \chi_{\text{DR16Ly}\alpha\text{-QSO}}^2, \end{aligned} \quad (\text{C20})$$

Here, the DR12, DR16 LRG and DR16 QSO data χ_i^2 are given in the form of $\chi_i^2 = (\mathbf{w}_i - \mathbf{d}_i)^T \cdot \mathbf{Cov}_i^{-1} \cdot (\mathbf{w}_i - \mathbf{d}_i)$. And, the vector \mathbf{d}_i is the observational data of the i th-type data set from Table 5, \mathbf{w}_i is the prediction for these vectors in a given cosmological model, and \mathbf{Cov}_i is the covariance matrix of different BAO data set.

C.3. OHD

In this paper, we use the most recent 32 OHD points summarized in Table 6. And the best-fitting parameters are obtained by minimizing this quantity

Table 5. BAO measurements used in our work.

Dataset	z_{eff}	Observable	Measurement	Reference
MGS	0.15	D_V/r_d	4.466 ± 0.168	Ross et al. (2015)
DR12LRG	0.38	D_M/r_d	10.234	Alam et al. (2017)
	0.38	D_H/r_d	24.980	
	0.51	D_M/r_d	13.366	
	0.51	D_H/r_d	22.317	
	0.698	D_M/r_d	17.858	
DR16LRG	0.698	D_H/r_d	19.326	Gil-Marín et al. (2020)
	0.845	D_V/r_d	18.33 ± 0.62	
DR16ELG	0.845	D_V/r_d	18.33 ± 0.62	de Mattia et al. (2021)
DR16QSO	1.48	D_M/r_d	30.6876	Neveux et al. (2020)
	1.48	D_H/r_d	13.2609	
DR16Ly α – Ly α	2.33	D_M/r_d	37.6 ± 1.9	du Mas des Bourboux et al. (2020)
	2.33	D_H/r_d	8.93 ± 0.28	
DR16Ly α – QSO	2.33	D_M/r_d	37.3 ± 1.7	
	2.33	D_H/r_d	9.08 ± 0.34	

$$\chi_{H(z)}^2 = \sum_{i=1}^{32} \frac{(H_{\text{obs},i} - H_{\text{th},i})^2}{\sigma_{H_i}^2}, \quad (\text{C21})$$

where $\sigma_{H_i}^2$ is the error of the i -th measurement.

Table 6. The compilation of OHD (in units of $\text{km s}^{-1}\text{Mpc}^{-1}$) and their errors σ_H at redshift z .

z	$H(z)$	σ_H	Reference	z	$H(z)$	σ_H	Reference
0.07	69.0	19.6	Zhang et al. (2014)	0.4783	80.9	9.0	Moresco et al. (2016)
0.1	69.0	12.0	Simon et al. (2005)	0.48	97.0	60.0	Stern et al. (2010)
0.12	68.6	26.2	Zhang et al. (2014)	0.5929	104.0	13.0	Moresco et al. (2012)
0.17	83.0	8.0	Simon et al. (2005)	0.6797	92.0	8.0	Moresco et al. (2012)
0.1791	75.0	4.0	Moresco et al. (2012)	0.75	98.8	33.6	Borghi et al. (2022)
0.1993	75.0	5.0	Moresco et al. (2012)	0.7812	105.0	12.0	Moresco et al. (2012)
0.20	72.9	29.6	Zhang et al. (2014)	0.8754	125.0	17.0	Moresco et al. (2012)
0.27	77.0	14.0	Simon et al. (2005)	0.88	90.0	40.0	Stern et al. (2010)
0.28	88.8	36.6	Zhang et al. (2014)	0.9	117.0	23.0	Simon et al. (2005)
0.3519	83.0	14.0	Moresco et al. (2012)	1.037	154.0	20.0	Moresco et al. (2012)
0.3802	83.0	13.5	Moresco et al. (2016)	1.3	168.0	17.0	Simon et al. (2005)
0.4	95.0	17.0	Simon et al. (2005)	1.363	160.0	33.6	Moresco (2015)
0.4004	77.0	10.2	Moresco et al. (2016)	1.43	177.0	18.0	Simon et al. (2005)
0.4247	87.1	11.2	Moresco et al. (2016)	1.53	140.0	14.0	Simon et al. (2005)
0.4497	92.8	12.9	Moresco et al. (2016)	1.75	202.0	40.0	Simon et al. (2005)
0.47	89	34	Ratsimbazafy et al. (2017)	1.965	186.5	50.4	Moresco (2015)